

## Handling

Generate  $r_{ref}$  by prefilter from  $\delta_S$  and  $v$

Stationary gain

$$k_{rstat}(v) = \frac{v}{\ell[1 + (v/v_{CH})^2]}, \quad v_{CH}^2 = \frac{\mu c_R c_F \ell^2}{m(c_R \ell_R - c_F \ell_F)}$$

Relative degree  $\delta_S \rightarrow r$  is one

Relative degree  $\delta_S \rightarrow r_{ref}$  should also be one (avoid initial peak in  $r_{ref} - r$ )

Prefilter

$$\frac{r_{ref}(s)}{\delta_S(s)} = \frac{k_{rstat}(v)}{1 + 0.1s} \quad (6.5.18)$$

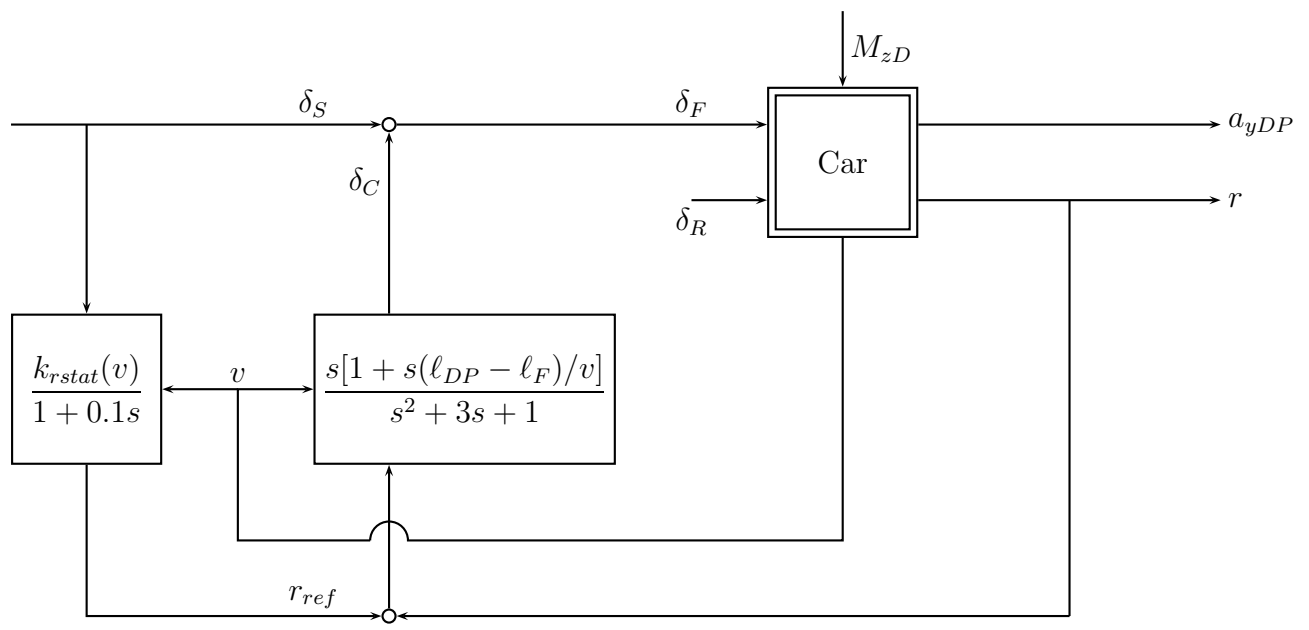


Figure 6.26. Robust unilateral decoupling by feedback of  $r$  to  $\delta_C$ .

Immediate reaction after step  $\delta_S$  is as in conventional car.

## Fading effect

Driver assistance important for 0.5 to 1 second after disturbance torque. Then corrective steering angle  $\delta_C$  should return to zero.

Steady state response as in conventional car, i.e.  $\delta_{Cstat} = 0$ .

Decoupling controller

$$\frac{1 + s(\ell_{DP} - \ell_F)/v}{s}$$

Replace integrator  $1/s$  by fading integrator

$$\frac{1}{s} \rightarrow \frac{s}{s^2 + 3s + 1}$$

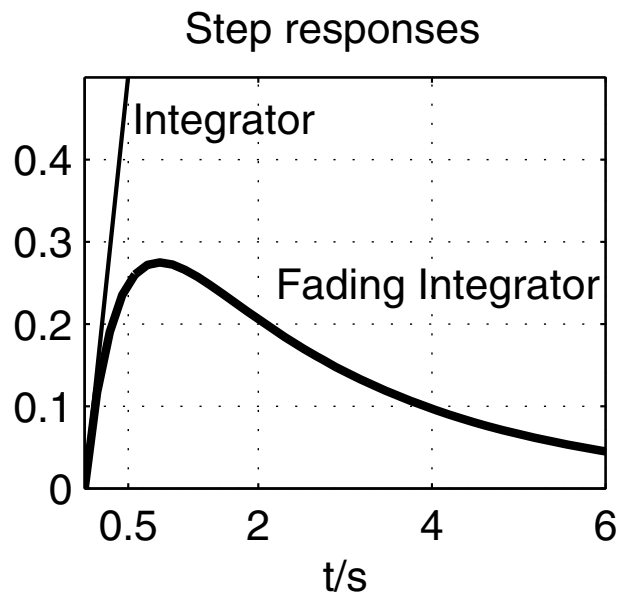


Figure 6.27. The initial response of the fading integrator is the same as that of the integrator.

## Conclusions

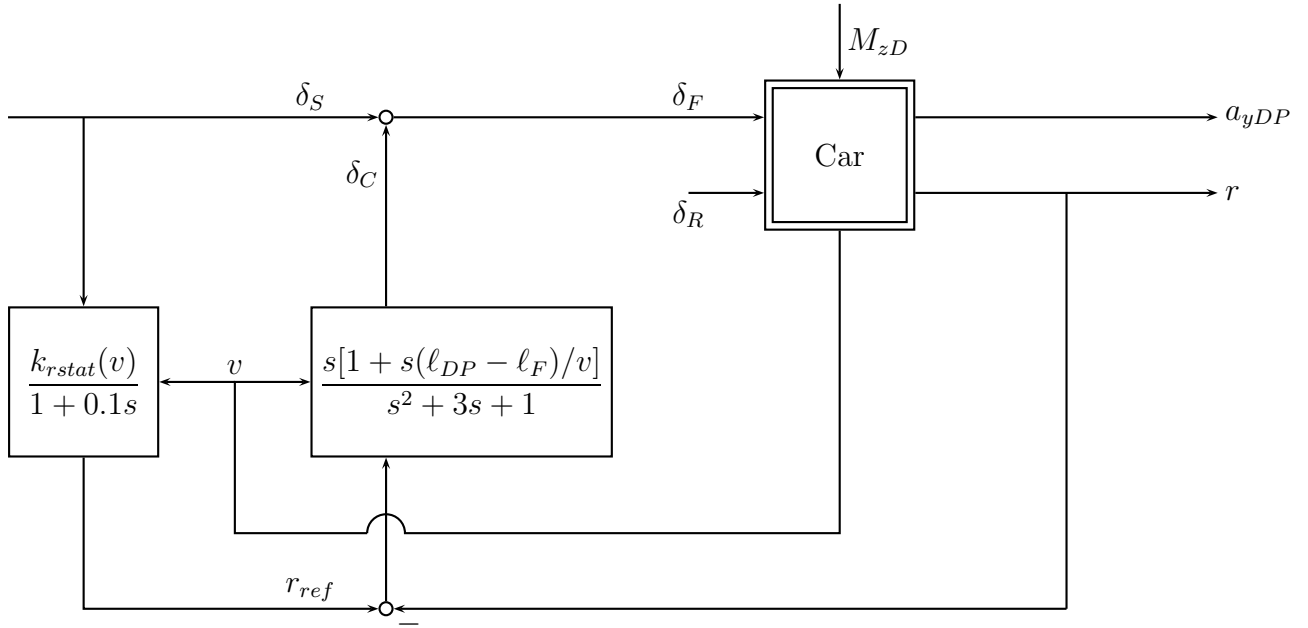


Figure 6.26. Robust unilateral decoupling by feedback of  $r$  to  $\delta_C$ .

- Initial and final reaction like conventional car.
- Transients are decoupled for first 0.5 to 1 second, i.e.  $r$  non-observable from  $a_{yDP}$ ,  $a_{yDP}$  is driver controlled for path tracking  $r$  is automatically controlled.
- Reduced yaw damping  $D(v)$  can be recovered by feedback  $r \rightarrow \delta_R$ .
- Controller parameters derived structurally  
Assignment only for  $D(v)$ .

## Practical constraints

- i. No rear-wheel steering,
- ii. Linear actuator dynamics cause phase delay,
- iii. Actuator rate limits, prevent limit cycles.

Feedback from  $r_{dec}$  to  $\delta_S$  destroys decoupling.

However factorization may be preserved, it allows to symbolically calculate and assign yaw damping  $D_{des}(v)$ .

*Theorem 6.12 (Ackermann)*

A second feedback loop

$$\delta_S(s) = \delta_{Sref}(s) - \left[ 2D_{des}(v) \sqrt{\frac{m\ell_{DP}}{\mu c_R} - \frac{\ell_R + \ell_{DP}}{v}} \right] \frac{1 + T_R s}{1 + T_F s} r_{dec}(s),$$

with

$$T_R = \frac{mv\ell_R}{\mu c_F \ell}, \quad T_F = \frac{mv\ell_F}{\mu c_R \ell} \quad (6.6.2)$$

around the robustly decoupled system of Figure 6.25 assigns the desired yaw damping characteristic  $D_{des}(v)$  to the system. Both the natural frequency  $\omega_{0dec} = \sqrt{\mu c_R / m\ell_{DP}}$  and the lateral dynamics pole  $p_{lat}(s) = s + \mu c_F \ell / mv\ell_R$  are invariant under the feedback (6.6.1).

□

## *Proof of Theorem 6.12*

The proof proceeds in two steps:

1. It is shown that the control law

$$\delta_S(s) = \delta_{Sref}(s) - (D_{des}(v) - D_{dec}(v))\omega_{0dec} \frac{2m\ell_R}{\mu C_F \ell} \frac{p_{lat}(s)}{n_{ardec}(s)} r_{dec}(s)$$

assigns the desired  $D_{des}(v)$ .

2. It is shown by substitution of  $\omega_{0dec}$  and  $d_{dec}$  that (6.6.3) is equal to (6.6.1), (6.6.2).

In the first step, the loop is closed with the plant

$$r_{dec}(s) = \frac{n_{Sadec}(s)n_{ardec}(s)}{p_{lat}(s)p_{yaw}(s)} \delta_S(s). \quad (6.6.4)$$

A double cancellation of the two stable first order polynomials  $p_{lat}(s)$  and  $n_{ardec}(s)$  occurs, and the closed-loop characteristic polynomial is

$$p(s) = p_{lat}(s)n_{ardec}(s) \left[ p_{yaw}(s) + (D_{des}(v) - D_{dec}(v)) \frac{2m\ell_R}{\mu C_F \ell} \omega_{0dec} n_{sadec}(s) \right]$$

With  $p_{yaw}(s)$  from (6.5.7) and  $n_{Sadec}$  from (6.5.10), the term in square brackets becomes

$$\begin{aligned} & s^2 + 2D_{dec}(v) \omega_{0dec} s + \omega_{0dec}^2 + (D_{des}(v) - D_{dec}(v)) \frac{2m\ell_R}{\mu c_F \ell} \omega_{0dec} \frac{\mu c_F \ell}{m\ell_R} s \\ & = s^2 + 2D_{des}(v) \omega_{0dec} s + \omega_{0dec}^2. \end{aligned}$$

It has the desired damping characteristic  $D_{des}(v)$  and the unchanged natural frequency  $\omega_{0dec}$ . Also, the factor  $p_{lat}(s)$  of  $p(s)$  is unchanged.

In the second step,  $\omega_{0dec}$  from (6.5.8) and  $D_{dec}(v)$  from (6.5.9) is substituted in the control law (6.6.3) to obtain

$$\delta_S(s) = \delta_{Sref}(s) - \left( D_{des}(v) + \frac{\ell_R + \ell_{DP}}{2v} \sqrt{\frac{\mu c_R}{m\ell_{DP}}} \right) 2 \sqrt{\frac{m\ell_{DP}}{\mu c_R} \frac{1 + T_R s}{1 + T_F s}},$$

which agrees with (6.6.1).

□

The dynamic part of the controller (6.6.1) is

$$\frac{1 + T_R s}{1 + T_F s}$$

For the typical understeering car  $c_R \ell_R - c_F \ell_F > 0$ , i.e.  $T_R > T_F$ , the additional controller has high-pass behavior (lead-lag filter).

## Limit cycles

Experiments with feedback of  $r$  and  $a_{yDP}$  showed oscillations at low speed.

Analysis: Limit cycles due to rate limitation.

Plant: BMW 735 i single-track model

- + second order actuator dynamics
- + robust decoupling
- + negative feedback of  $a_{yDP}$  with gain 1.8.

Nyquist plot with negative-inverse describing function of rate saturation.

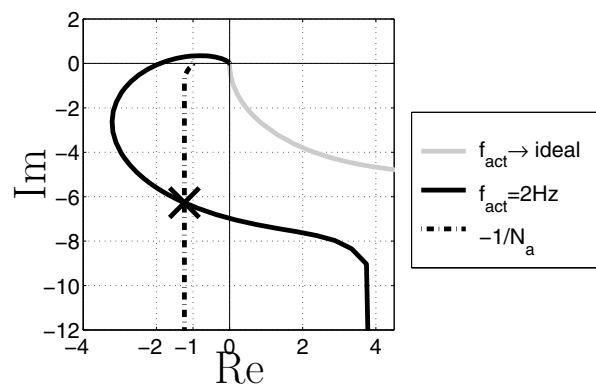


Figure 6.28. Reconstruction of steering limit cycles at  $v = 5$  m/s,  $\mu = 1$  with additional feedback of lateral acceleration

Limit cycle with  $f = 1.26$  Hz, i.e.  $\omega = 2\pi 1.26$  Radian  $s^{-1}$

$$R/A = 0.97 s^{-1}$$

in agreement with experimental results.

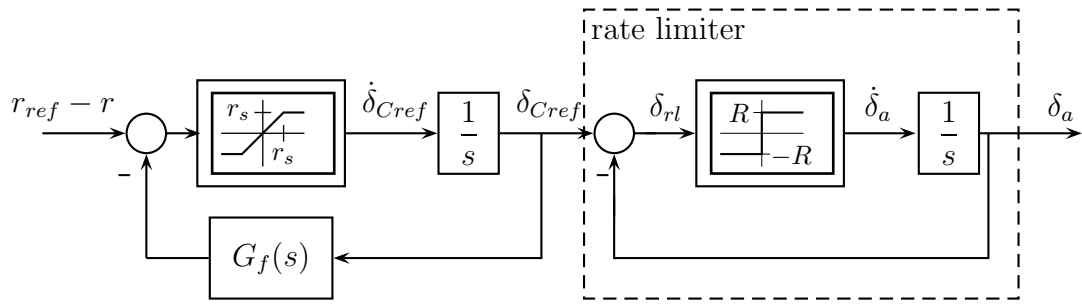


Figure 6.34. Nonlinear controller enhancement of the fading integrator

### Specification of actuator bandwidth

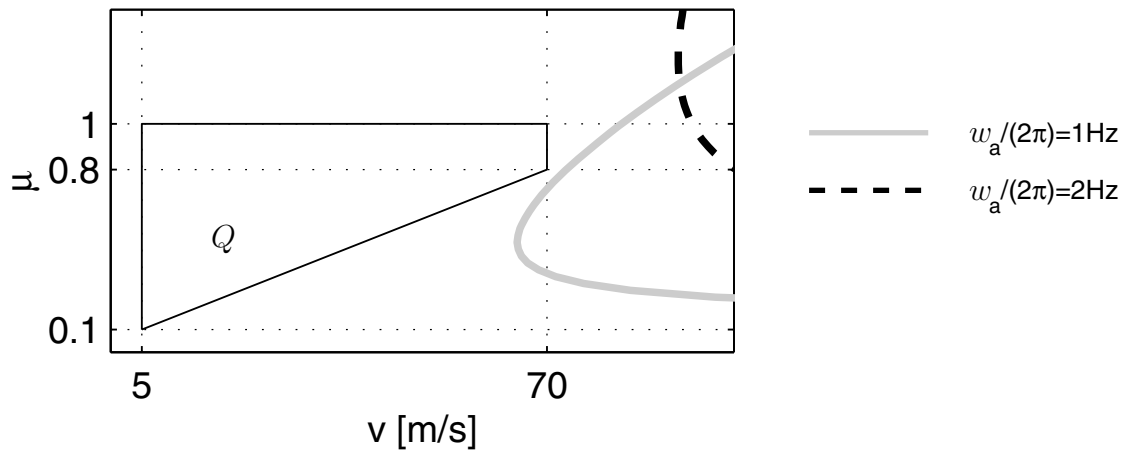


Figure 6.35. Limit cycle  $\Theta$ -stability boundaries in the  $(v, \mu)$ -plane

## Automatic car steering

Reference:

Guiding wire or permanent magnets on lane center, or video camera image processing.

Controller input is deviation from lane center

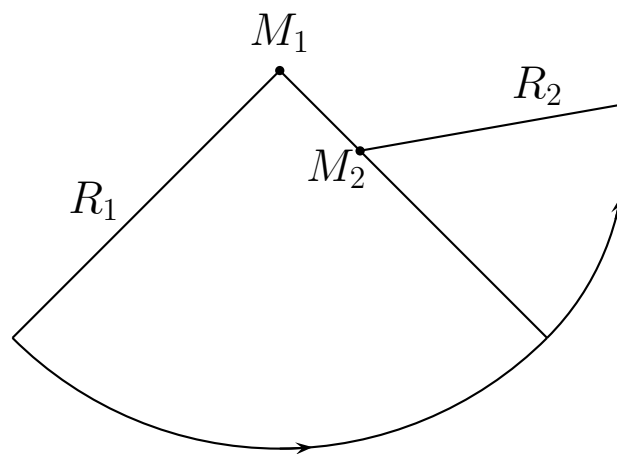


Figure 6.77. The reference path is comprised of circular arcs.

Vehicle motion modelled as small deviation from stationary circular path

Extend single-track model by yaw angle and lateral displacement.

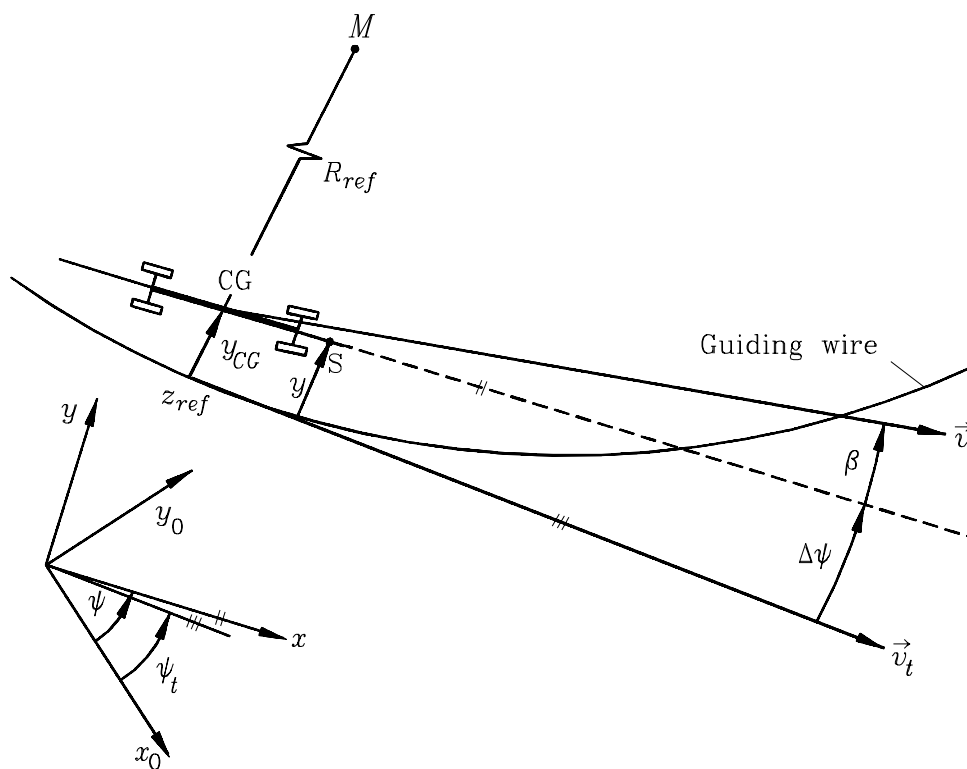


Figure 6.78. Vehicle heading and measured displacement  $y$  from the guiding wire in stationary circular cornering.

$$\dot{y}_{CG} = v(\beta + \Delta\psi) \quad (6.8.1)$$

$$\dot{y} = v(\beta + \Delta\psi) + \ell_S r \quad (6.8.2)$$

$$\begin{aligned} \Delta\dot{\psi} &= \dot{\psi} - \dot{\psi}_t \\ &= r - r_{st} \\ &= r - vQ_{ref} \end{aligned}$$



$$y(s) = \frac{n(s)}{(a_0 + a_1s + s^2)s^2} \delta_F(s) \quad (6.8.5)$$

$$n(s) = b_2s^2 + b_1s + b_0 \quad (6.8.7)$$

$$b_2 = \frac{\mu c_F \ell \ell_S}{m \ell_R \ell_{DP}} + v$$

$$b_1 = \frac{\mu c_F}{m \ell_{DP}} \left[ v + \frac{\mu c_R \ell}{m v \ell_R \ell_F} \left( \frac{\ell \ell_S}{\ell_R \ell_F} + 1 \right) \right]$$

$$b_0 = \frac{\mu^2 c_R c_F \ell^2}{m^2 \ell_F \ell_R \ell_{DP}}$$

$$a_0 = \frac{\mu}{m \ell_R \ell_{DP}} \left[ \frac{\mu c_F c_R \ell^2}{m v^2} + c_R \ell_R - c_F \ell_F \right]$$

$$a_1 = \frac{\mu}{m v} \left[ c_R + c_F + \frac{c_R \ell_R^2 + c_F \ell_F^2}{\ell_R \ell_{DP}} \right]$$

**Controllability:** Same condition as for single-track model

**Observability** from  $y$

$$\begin{bmatrix} \mathbf{c}^T \\ \mathbf{c}^T \mathbf{A} \\ \mathbf{c}^T \mathbf{A}^2 \\ \mathbf{c}^T \mathbf{A}^3 \end{bmatrix} = \begin{bmatrix} 0 & 0 & 0 & 1 \\ v & \ell_S & v & 0 \\ o_{31} & o_{32} & 0 & 0 \\ o_{41} & o_{42} & 0 & 0 \end{bmatrix}$$

columns 3 and 4 yield rank 2 for  $v \neq 0$ .

columns 1 and 2 increase rank to four for

$$o_{31}o_{42} - o_{32}o_{41} = -\frac{\mu^2 \ell^2}{m^2 v \ell_R \ell_{DP}} \neq 0$$

$\Rightarrow \mu \neq 0$ .

Observability decreases for high  $v$ .

**Observability** from  $r$

$$\det \begin{bmatrix} \mathbf{c}^T \\ \mathbf{c}^T \mathbf{A} \end{bmatrix} = \det \begin{bmatrix} 0 & 1 \\ a_{21} & a_{22} \end{bmatrix} = -a_{21} = \frac{-\mu(c_R \ell_R - c_F \ell_F)}{m \ell_R \ell_{DP}}$$

observability independent of  $v$ .

Additional measurement of  $r$  improves observability for higher  $v$ .

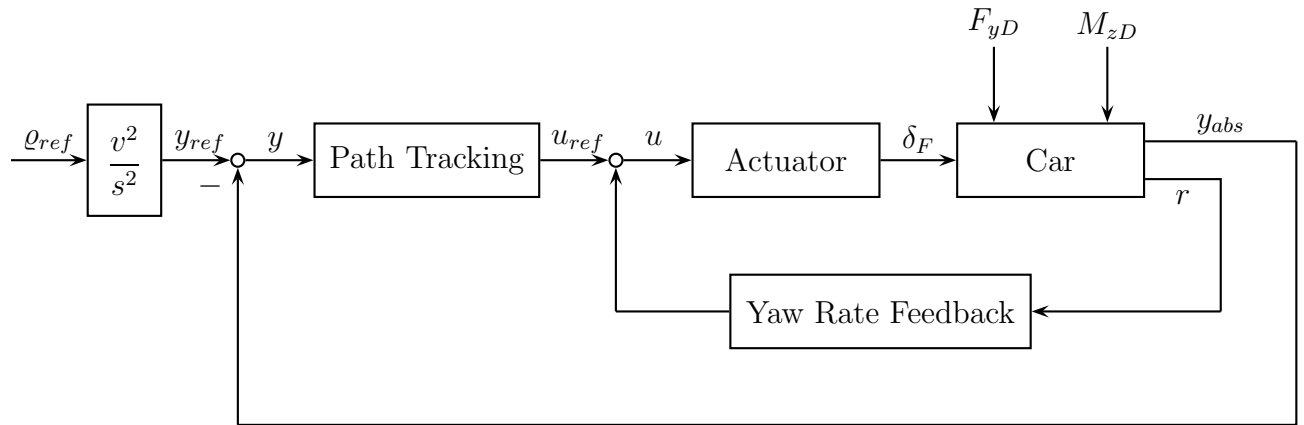


Figure 6.81. Feedback structure for automatic car steering.

Industry experiments began in early 1980's, rate sensors were expensive gyros.

Second displacement sensor:  $y_R$

Feedback structures

- 1) MAN  $y$  and  $\delta_F$  for feedback,  $v$  for gain scheduling,  $y_R$  for curvature estimation.
- 2) Daimler-Benz
  - a)  $y, y_R, \delta_F$  for feedback
  - b) only  $y$  for feedback
- 3) Proposal Ackermann (1990)
 

$y$  and  $r$  for feedback
- 4) PATH  $y, y_R$  and  $r$  for feedback, curvature  $q_{ref}$  with preview encoded in magnets.

Hydraulic actuator without position feedback

Transfer function  $1/s$

$$G(s) = \frac{b(s^2 + b_1s + b_0)}{(s^2 + a_1s + a_0)s^3} \quad (6.8.14)$$

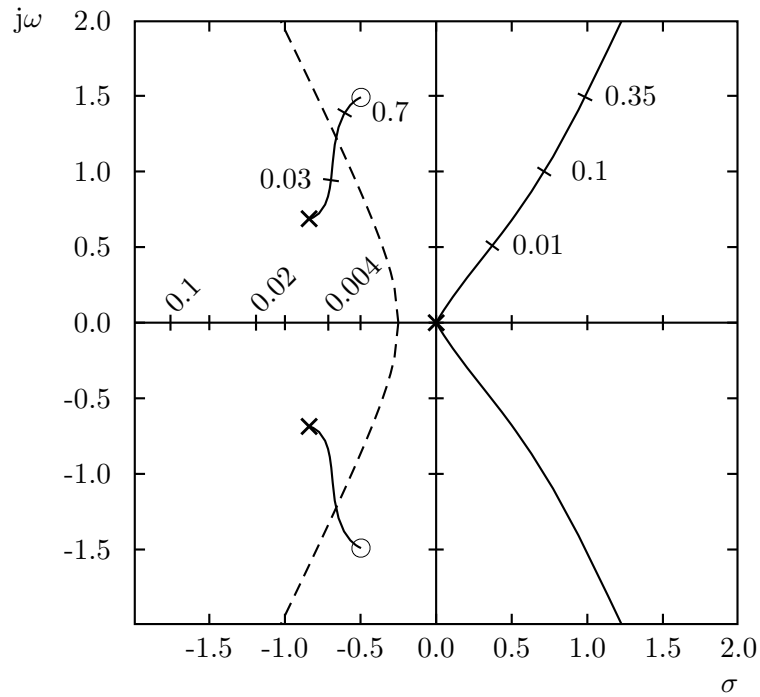


Figure 6.83. Root locus of an automatic car steering system with proportional feedback of the front displacement from the guideline.

## Linear controller structure

Attract RHP branches by two fine-tuned controller zeros

$$\delta_F(s) = \frac{k_1 + k_2s + k_3s^2}{(1 + s/\omega_0 + s^2/\omega_0^2)(1 + s/\omega_0)}y(s) \quad (6.8.15)$$

Relative degree one to reduce high-frequency noise from guiding wire reference.

Low frequency interpretation:

$k_1$  proportional

$k_2$  derivative

$k_3$  second dervative

Controller structure is lean: Tune only  $k_1, k_2, k_3, \omega_0$ .

## Specifications

- i) Less than 2cm track deviation on a straight lane without wind, less than 15cm under sidewind of 20m/sec.
- ii) Less than 15cm peak deviation after entering a curve.
- iii) Observing the  $|\dot{\delta}| \leq 23$  degree/sec steering rate constraint also in the worst case of entering a narrow parking bay.
- iv) Smooth transition from manual to automatic control.
- v) Keep the lateral acceleration below  $2\text{m/sec}^2$  for passenger comfort.

can be met by  $\Gamma$ –stability

$$\left(\frac{\sigma}{0.35}\right)^2 - \left(\frac{\omega}{1.75}\right)^2 = 1, \sigma < -0.35$$

## Design steps

$$\delta_F(s) = \frac{k_1 + k_2s + k_3s^2}{(1 + s/\omega_0 + s^2/\omega_0^2)(1 + s/\omega_0)}y(s) \quad (6.8.15)$$

Start with high bandwidth  $\omega_0 = 100$ .

Stepwise reduction narrows  $\Gamma$ –stable  $k_1$ –range.

Fix  $\omega_0 = 25, k_1 = 0.6$

Map  $\partial\Gamma$  to  $(k_2, k_3)$ –plane

Intersect admissible regions for four vertices of  $Q$ .

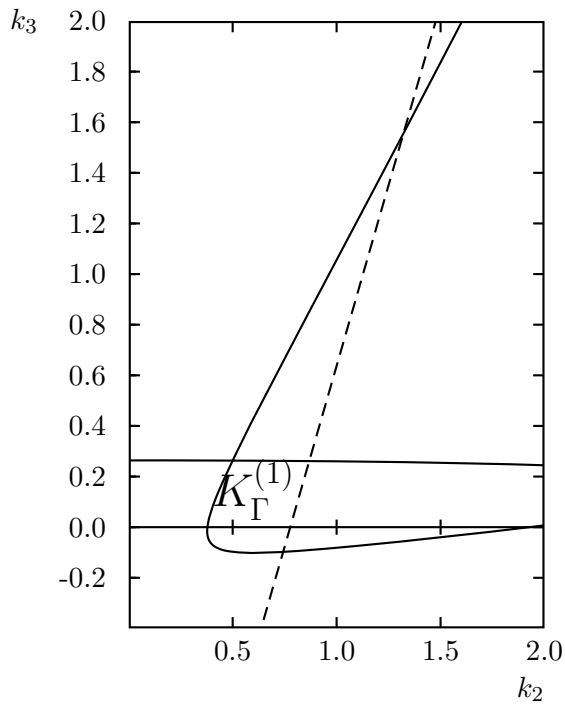


Figure 6.84. Set of  $\Gamma$ -stabilizing controllers for  $\tilde{m} = 9950$  [kg],  $v = 3$  [m · s<sup>-1</sup>],  $\omega_0 = 25$ ,  $k_1 = 0.6$ .

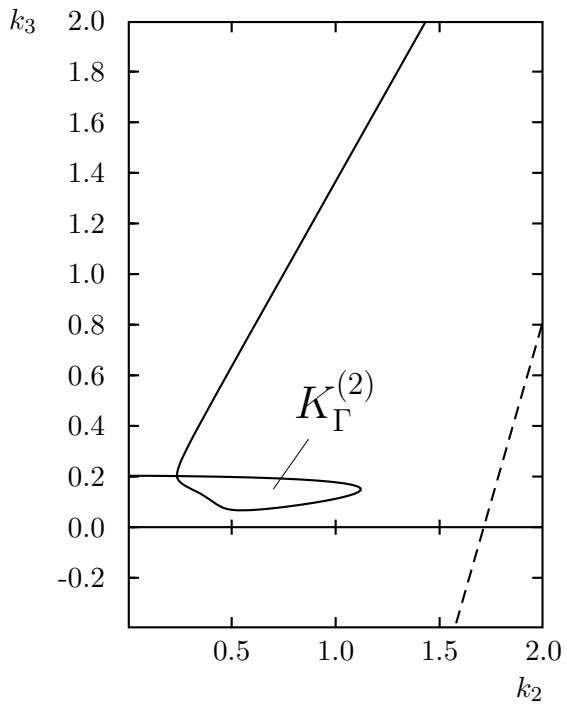


Figure 6.85. Set of  $\Gamma$ -stabilizing controllers for  $\tilde{m} = 9950$  [kg],  $v = 20$  [m · s<sup>-1</sup>],  $\omega_0 = 25$ ,  $k_1 = 0.6$ .

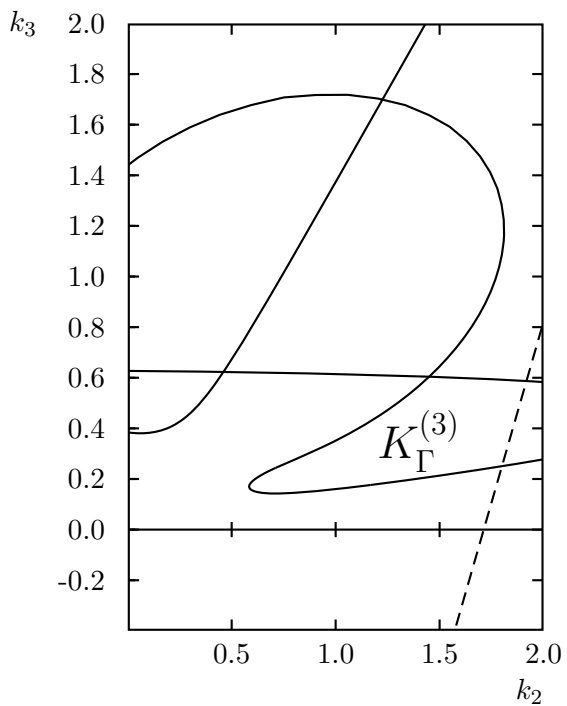


Figure 6.86. Set of  $\Gamma$ -stabilizing controllers for  $\tilde{m} = 32000$  [kg],  $v = 20$  [m · s<sup>-1</sup>],  $\omega_0 = 25$ ,  $k_1 = 0.6$ .

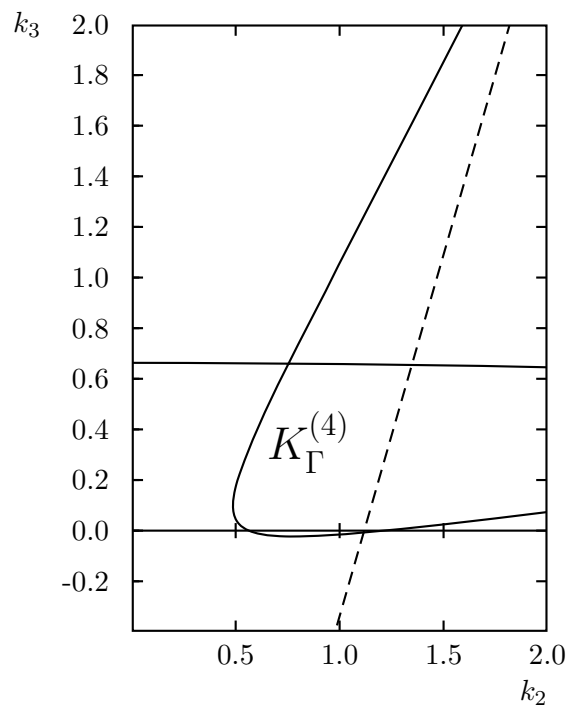


Figure 6.87. Set of  $\Gamma$ -stabilizing controllers for  $\tilde{m} = 32000$  [kg],  $v = 3$  [m  $\cdot$  s $^{-1}$ ],  $\omega_0 = 25$ ,  $k_1 = 0.6$ .

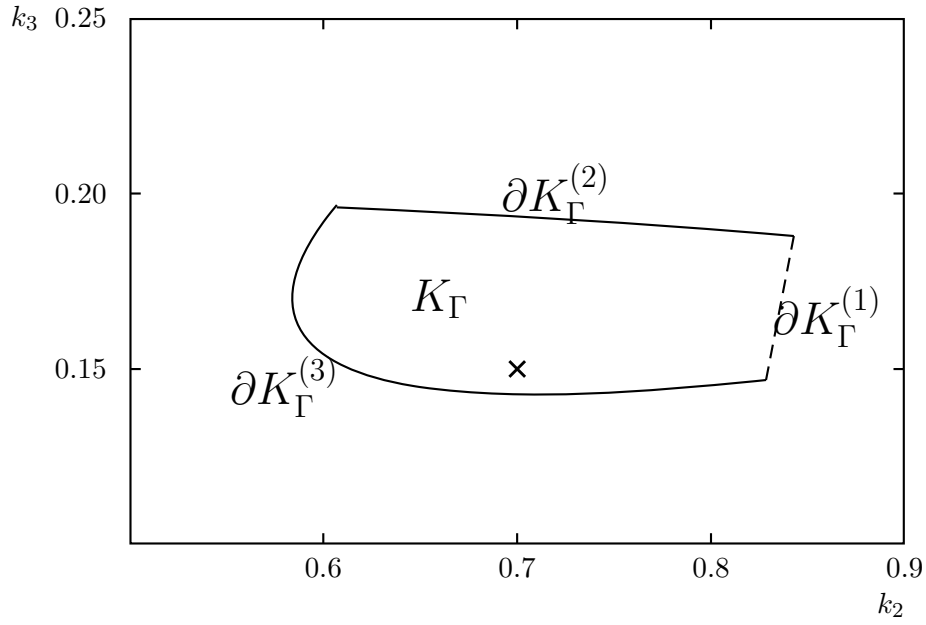


Figure 6.88. Simultaneously stabilizing set for the extremal plants for  $\omega_0 = 25$ ,  $k_1 = 0.6$ .

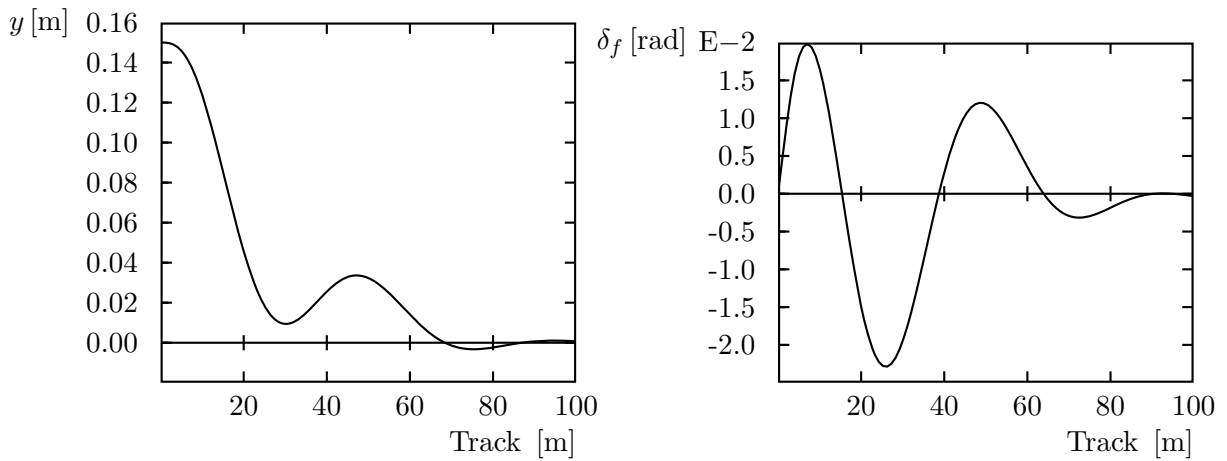


Figure 6.89. Simulation of a transition from manual to automatic steering for  $v = 20 \text{ [m} \cdot \text{s}^{-1}]$  and  $\tilde{m} = 32000 \text{ [kg]}$ .

## Closed-Loop Characteristic Polynomial

$$p(s, m, v) = \sum_{i=0}^8 a_i(m, v) s^i$$

Coefficients depend polynomially on parameters  $m$  and  $v$ .

$$\begin{aligned} a_0 &= 4.503 \cdot 10^{14} v^2 \\ a_1 &= 5.253 \cdot 10^{14} v^2 + 3.625 \cdot 10^{15} v \\ a_2 &= 5.699 \cdot 10^9 m v^2 + 1.126 \cdot 10^{14} v^2 + 4.299 \cdot 10^{15} v \\ a_3 &= 6.908 \cdot 10^9 m v^2 + 9.062 \cdot 10^{14} v + 4.203 \cdot 10^{15} \\ a_4 &= 1.445 \cdot 10^9 m v^2 + 1.680 \cdot 10^{10} m v + 3.362 \cdot 10^{14} \\ a_5 &= 1.563 \cdot 10^4 m^2 v^2 + 8.315 \cdot 10^5 m v^2 + 1.344 \cdot 10^9 m v + 1.345 \cdot 10^{13} \\ a_6 &= 1.25 \cdot 10^3 m^2 v^2 + 1.633 \cdot 10^4 m v^2 + 5.376 \cdot 10^7 m v + 2.690 \cdot 10^{11} \\ a_7 &= 50 m^2 v^2 + 1.075 \cdot 10^6 m v \\ a_8 &= m^2 v^2 \end{aligned}$$

$\Gamma$ -Stability Boundary:

Left-branch of hyperbola  $\left(\frac{\sigma}{0.35}\right)^2 - \left(\frac{\omega}{1.75}\right)^2 = 1$

## $\Gamma$ -Stabilität:

Alle Pole des geschlossenen Kreises links vom linken Ast der Hyperbel

$$\left(\frac{\sigma}{0.35}\right)^2 - \left(\frac{\omega}{1.75}\right)^2 = 1$$

Parametrierung

$$-\alpha(=\sigma) \leq -0.35$$

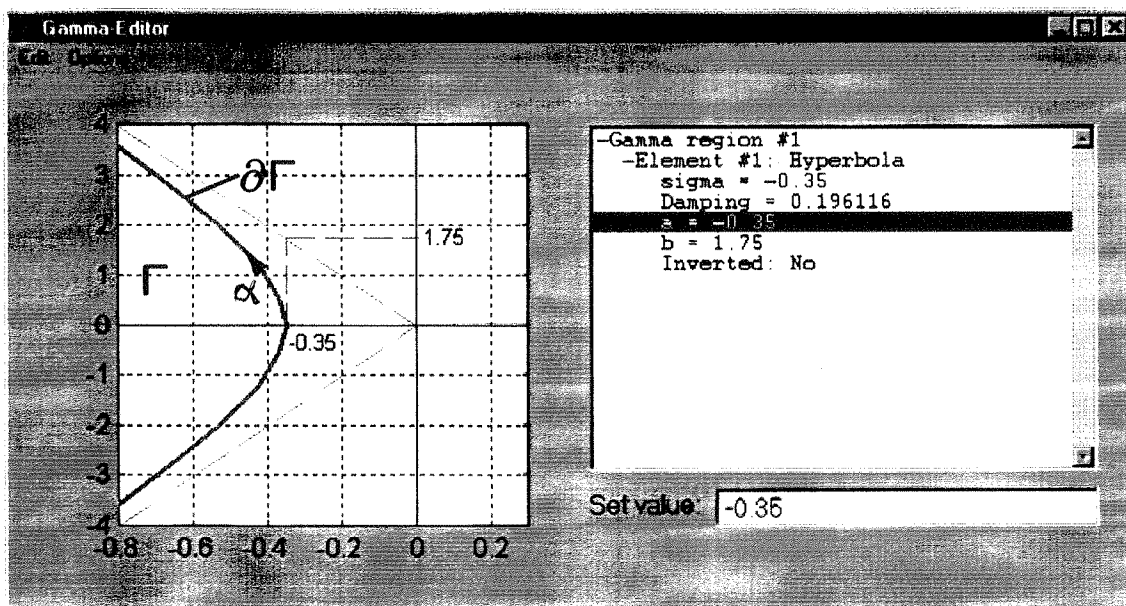


Abbildung von  $\partial\Gamma$  in die  $(v, \tilde{m})$ -Ebene

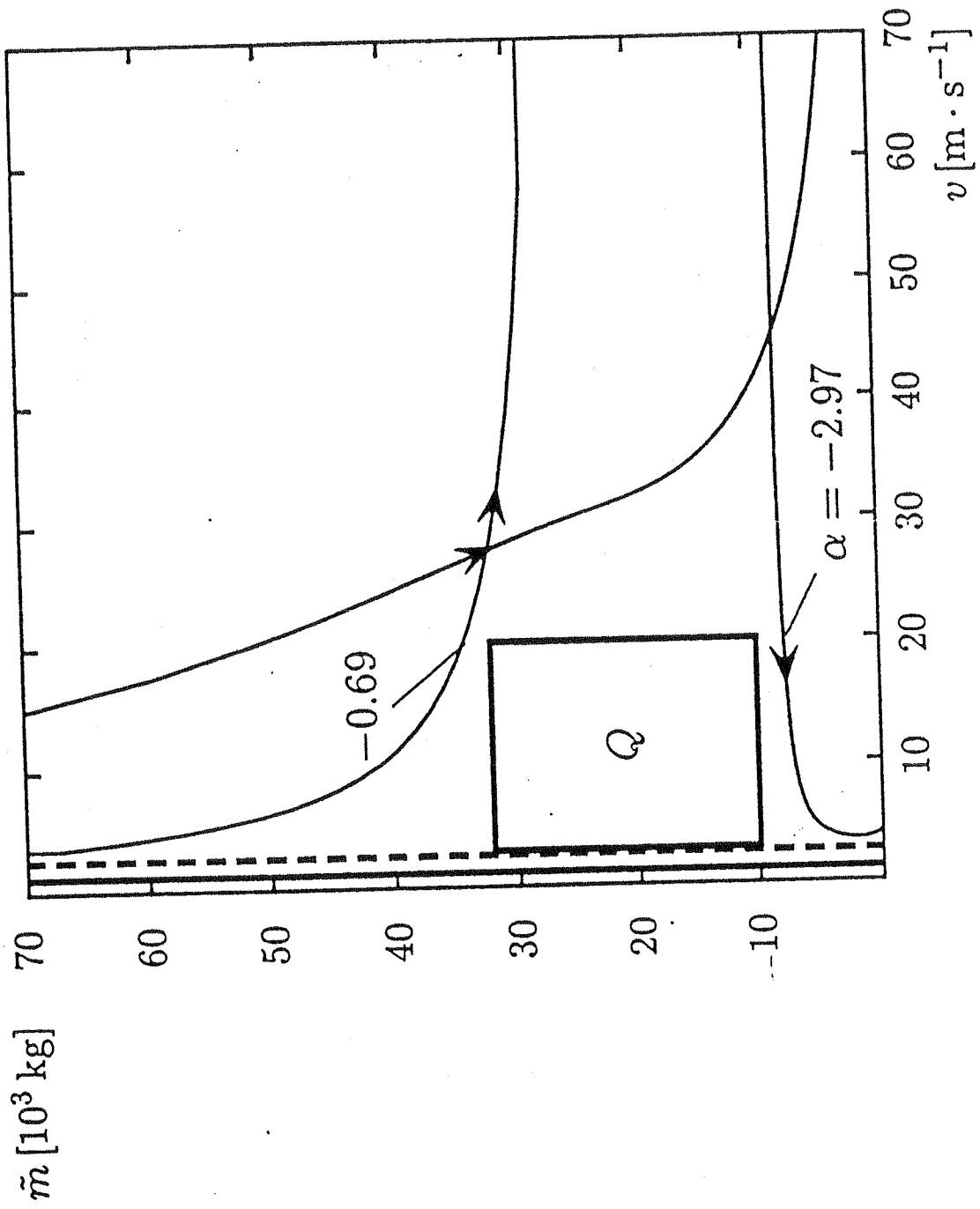


Abb. 9.4: Der spurgeführte Bus ist im Betriebsbereich  $Q$  robust  $\Gamma$ -stabil

## Improved accuracy by yaw rate feedback

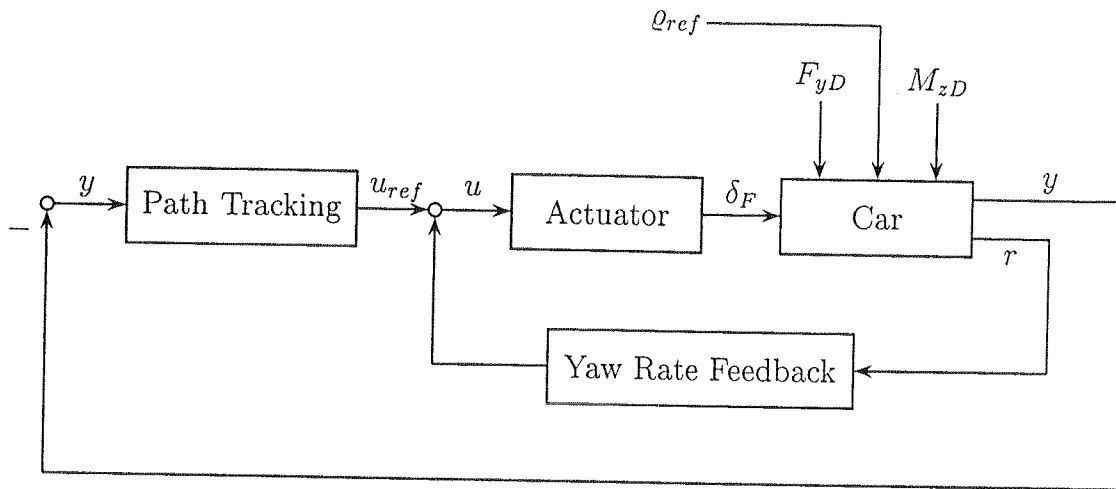


Fig. 6.84: Feedback structure for automatic car steering

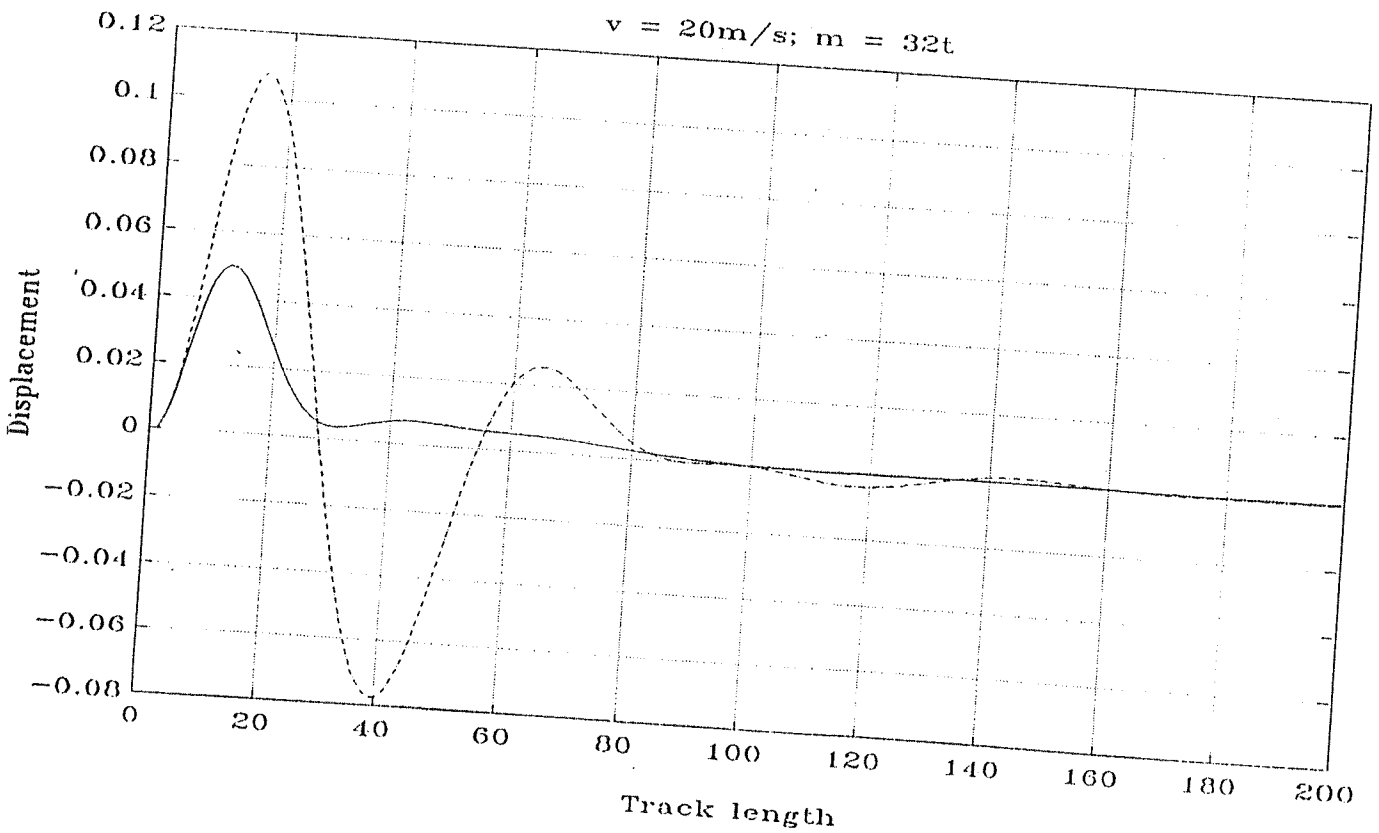
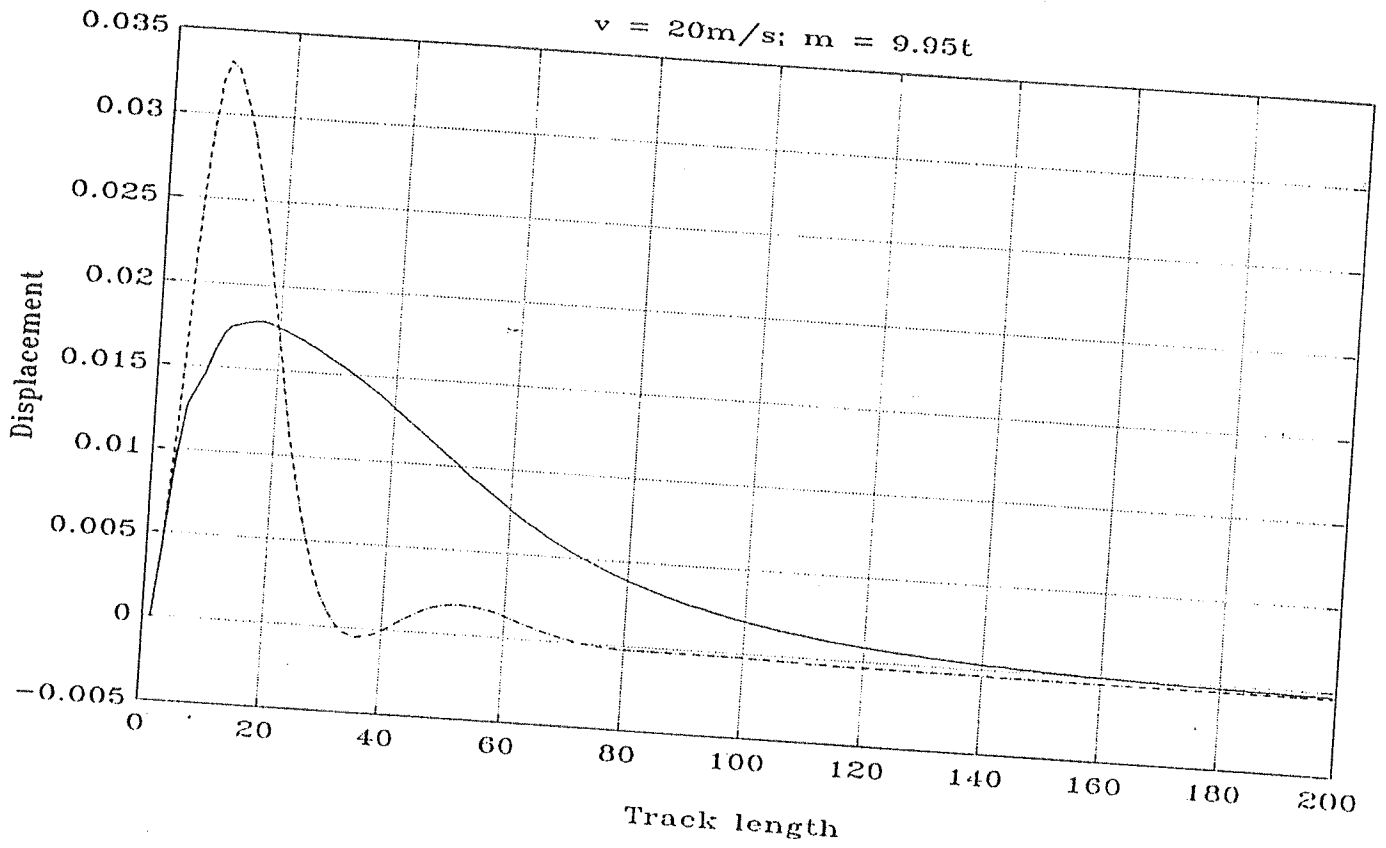
Use decoupling yaw rate feedback first, then redesign the controller for the modified plant with input  $u_{ref}$ .

All tracking errors are reduced by at least 50 %

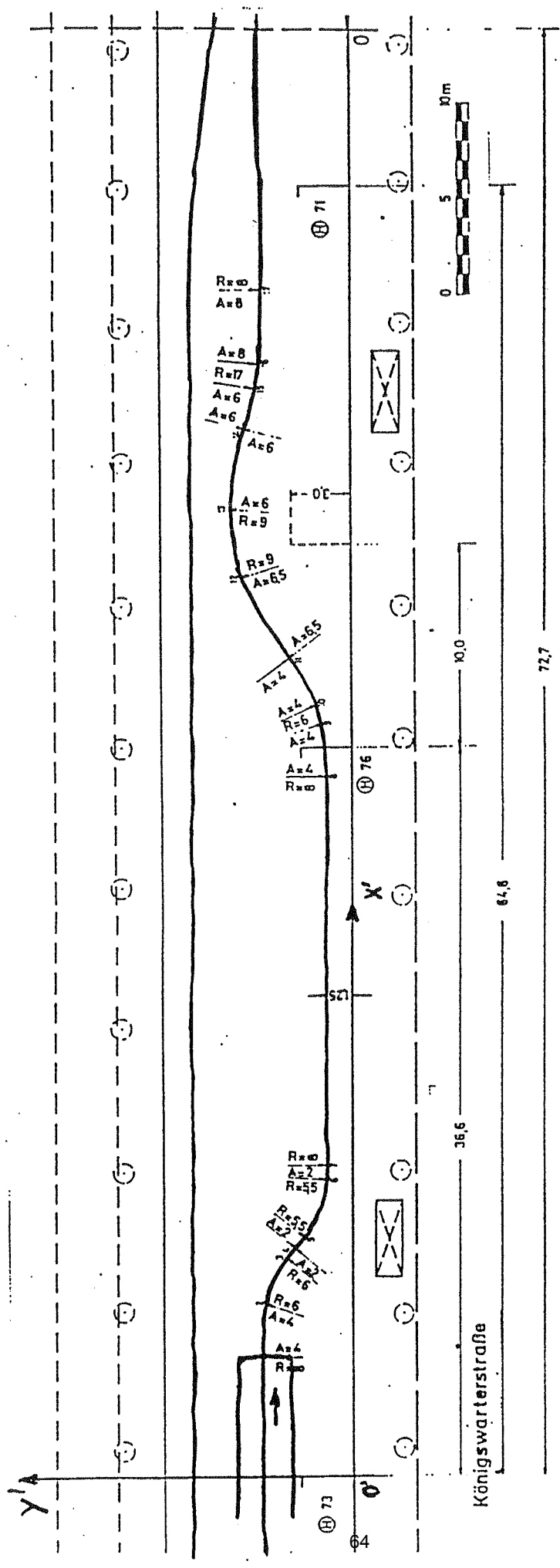
In the following simulations

..... controller with feedback of  $y$  only

—— controller with feedback of  $y$  and  $r$



TRANSITION FROM STRAIGHT LINE INTO CIRCLE

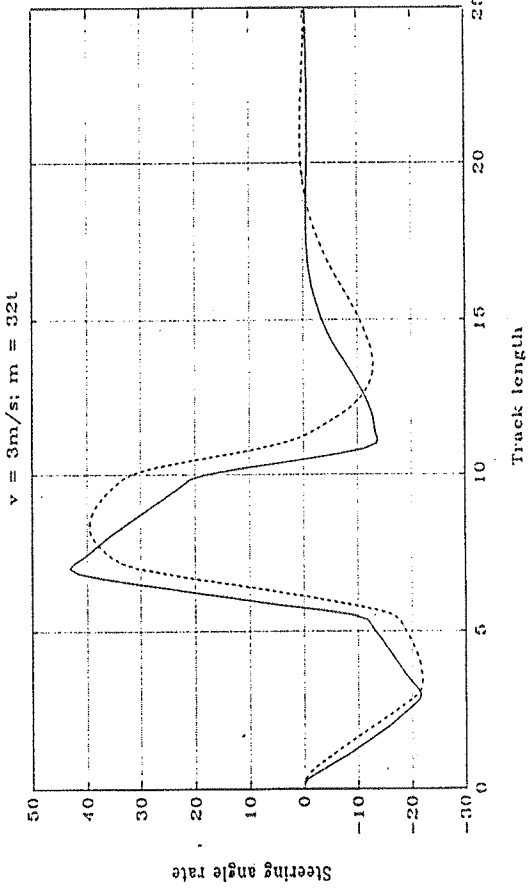
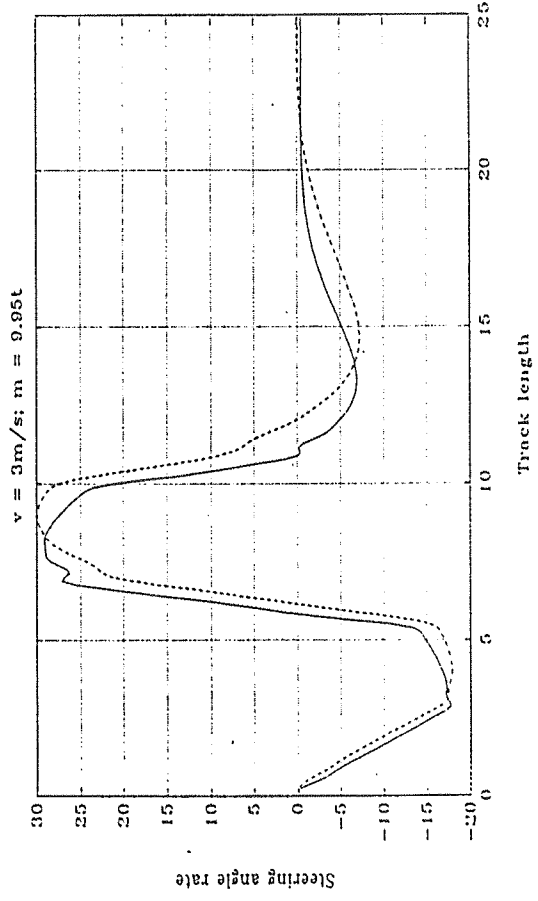
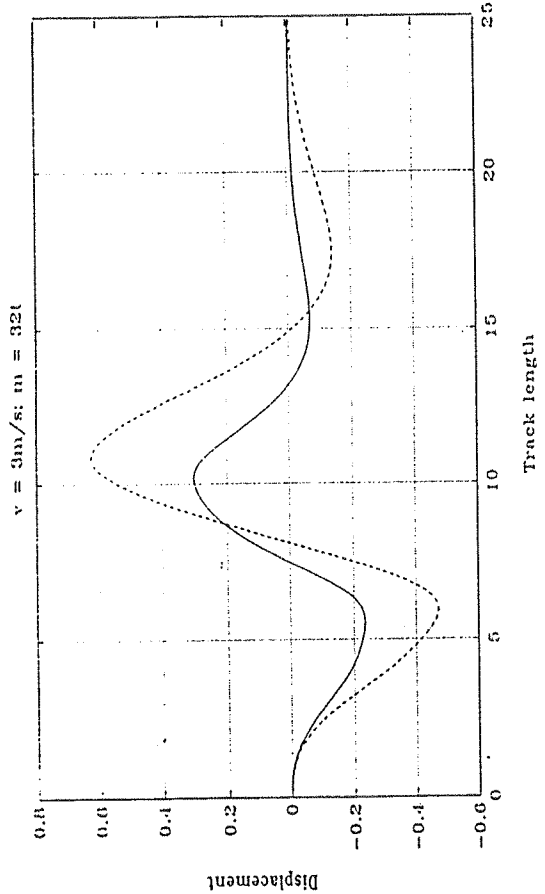
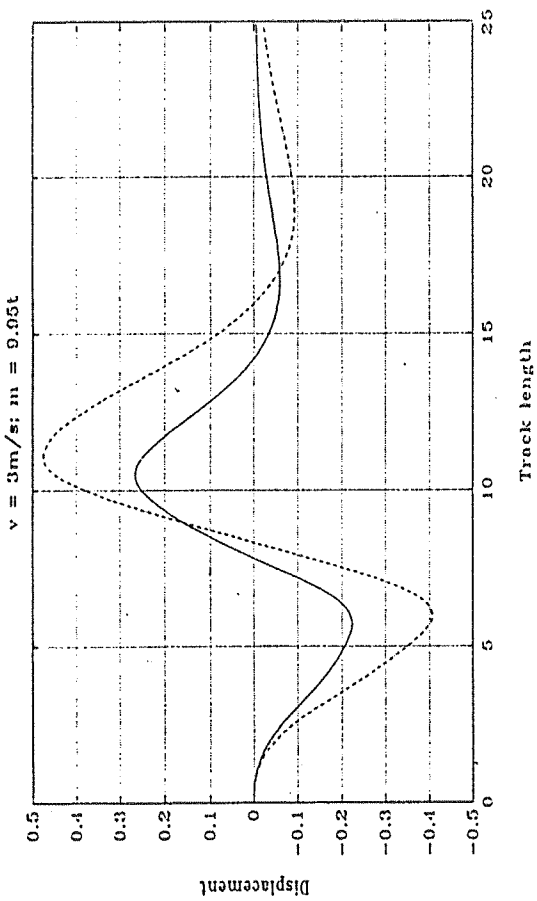


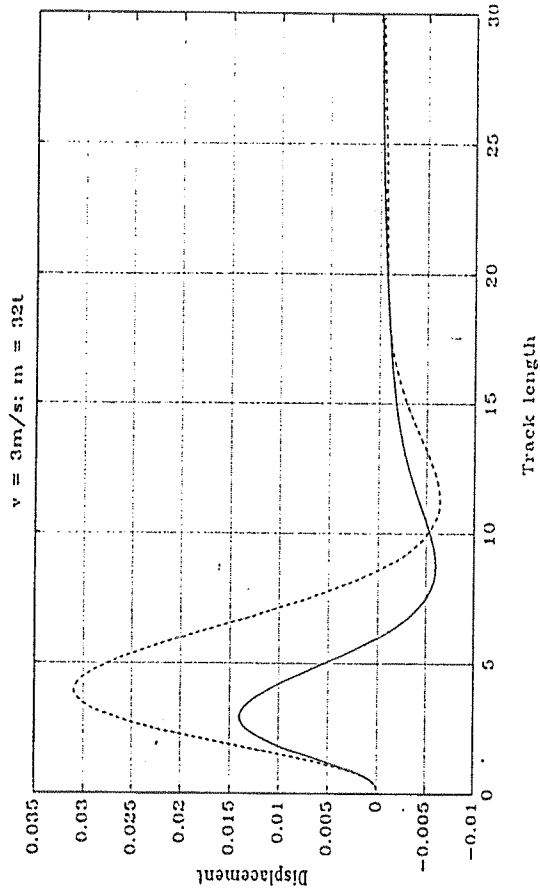
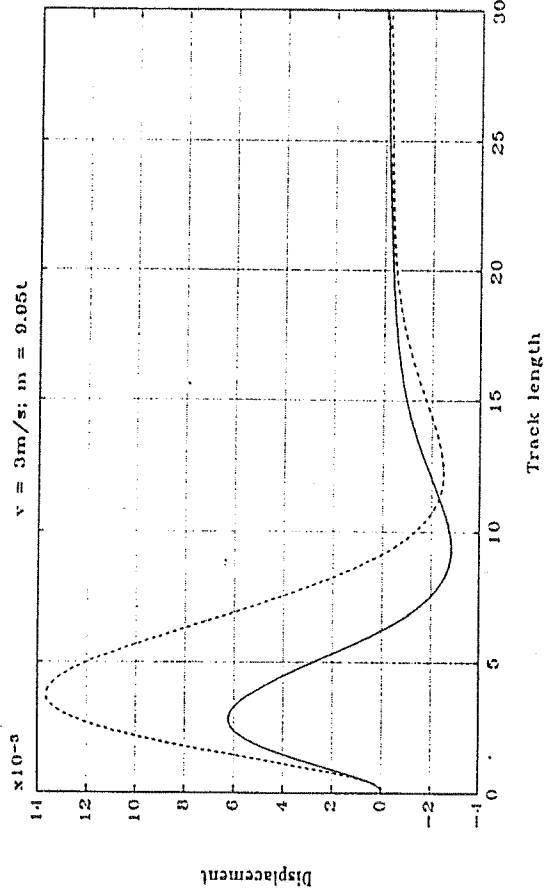
Forschung und  
Entwicklung

E6W 25985/5

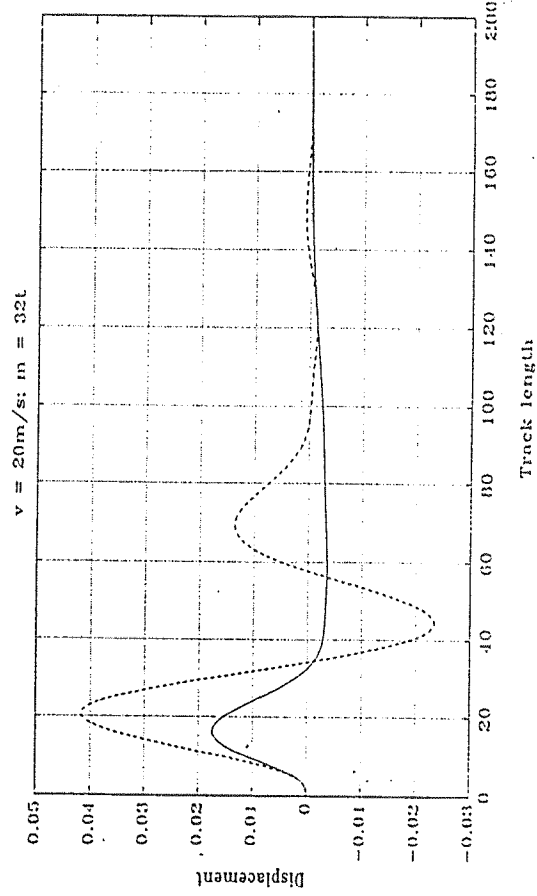
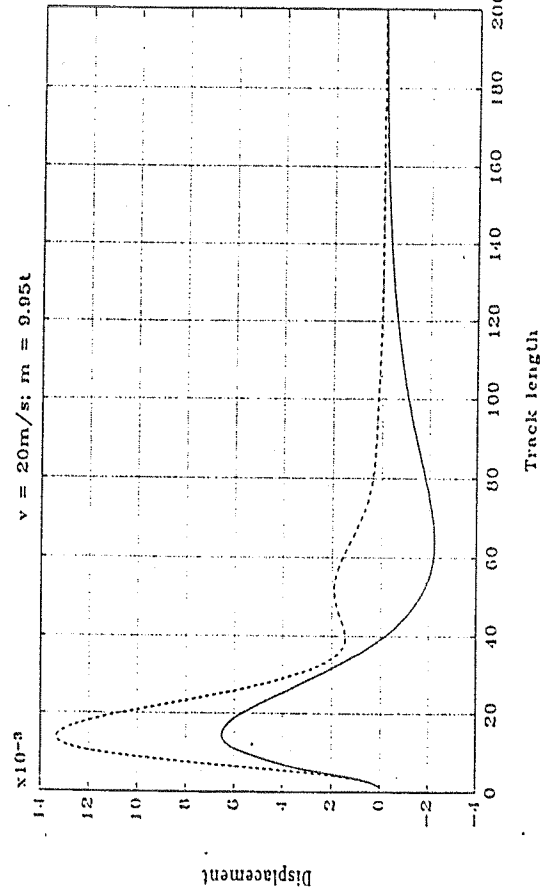
Sollkurs  
Fürth  
Haltestelle







99



SIDE WIND FORCE  $20\text{ms}^{-1} (1 - e^{-t/T})$ ,  $T=0.5\text{s}$

